Heliyon

Received:
21 September 2018
Revised:
22 November 2018
Accepted:
24 December 2018

Cite as: Jesús Barrera-Rojas, Luis González de la Vara, Emmanuel Ríos-Castro, Lourdes E. Leyva-Castillo, Carlos Gómez-Lojero. The distribution of divinyl chlorophylls *a* and *b* and the presence of ferredoxin-$NADP^+$ reductase in *Prochlorococcus marinus* MIT9313 thylakoid membranes.
Heliyon 4 (2018) e01100.
doi: 10.1016/j.heliyon.2018.e01100

The distribution of divinyl chlorophylls *a* and *b* and the presence of ferredoxin-$NADP^+$ reductase in *Prochlorococcus marinus* MIT9313 thylakoid membranes

Jesús Barrera-Rojas [a], Luis González de la Vara [b], Emmanuel Ríos-Castro [c], Lourdes E. Leyva-Castillo [a], Carlos Gómez-Lojero [a,*]

[a] *Departamento de Bioquímica, Centro de Investigación y Estudios Avanzados del IPN, Mexico*

[b] *Unidad Irapuato, Centro de Investigación y Estudios Avanzados del IPN, Mexico*

[c] *y LaNSE, Centro de Investigación y Estudios Avanzados del IPN, Mexico*

[*] Corresponding author.

E-mail address: cgomez@cinvestav.mx (C. Gómez-Lojero).

Abstract

The marine unicellular green cyanobacterium *Prochlorococcus marinus* MIT9313 belongs to the most abundant and photosynthetically productive genus of cyanobacteria in the oceans. This monophyletic genus use divinyl chlorophyll *a* (Chl a_2) and *b* (Chl b_2) to build the photosystems and the membrane-intrinsic Pcb-type antennae. We used the mild detergent n-dodecyl β D-maltopyranoside to solubilize the thylakoid membranes. Gel electrophoresis and sucrose gradient ultracentrifugation was then used to separate the complexes of the photosynthetic apparatus. The proteins and the pigments were identified by mass spectrometry. Protein complexes were characterized biochemically, and the distribution of Chl a_2 and Chl b_2 was determined. The photosynthetic apparatus was shown as supercomplexes formed by Photosystem II dimers with up to eight PcbB proteins; Photosystem I was present as trimers. A heterogeneous distribution of pigments was shown using sucrose gradient-enriched fractions with ratios of [Chl

https://doi.org/10.1016/j.heliyon.2018.e01100

b_2]/[Chl a_2] of 2.16 ± 0.13, 1.86 ± 0.08, and 2.61 ± 0.07, for Photosystem I, Photosystem II, and PcbB, respectively. These ratios of Chl *b*/*a* are without precedent in organisms with oxygenic photosynthesis. Diaphorase activity was measured in the fractions of the sucrose gradient. Gel electrophoresis, immunodetection, and mass spectrometry were used to conclude that the commonly soluble protein ferredoxin-$NADP^+$ reductase (FNR) is a membrane-anchored protein (probably associated to cytochrome b_6f complex) in the low-light adapted *Prochlorococcus marinus* MIT9313.

Keyword: Biochemistry

1. Introduction

The photosynthetic apparatus in oxygenic organisms include the peripheral light harvesting-antenna, photosystem I (PSI), photosystem II (PSII). The cytochrome b_6f complex couples the photosystems (PSs) in the "Z" scheme of electron transfer. In the photosystems, the light energy is transduced, which drives the electron flow across electron carriers in the thylakoid membrane to the final acceptor, ferredoxin. In the final step, electrons are transferred from ferredoxin to $NADP^+$ by ferredoxin-$NADP^+$ reductase (FNR). The light-driven electron flow generates a proton concentration gradient across the thylakoid membrane, which is used by ATP synthase to generate ATP. The peripheral light-harvesting antenna is the main component for the absorption and transfer of the light energy in the photosynthetic apparatus. During evolution, the antenna complexes were selected to absorb the part of the spectrum of light that arrives to the antenna, and to deliver efficiently the excitation energy to the reaction centers (RC) [1, 2].

The great structural diversity of the photosynthetic antenna is not surprising, because the only selective pressure it experience is the efficiency in absorption and transfer of the excitation energy to the RC. In most cyanobacteria, the peripheral light-harvesting antenna is coupled with an external giant complex, the phycobilisome [3]. In the so-called prochlorophytes: *Prochloron didemi* [4], *Prochlorothrix hollandica* [5], and *Prochlorococcus* spp. [6] it is formed by integral membrane proteins that are coupled with the photosystems.

Prochlorococcus is a diverse genus of marine cyanobacteria with environmental, trophic, and photosynthetic-productivity relevance [6, 7, 8]. *Prochlorococcus* cells are abundant in wide areas of oligotrophic ecosystems in the ocean [9, 10, 11]. Different ecotypes [12] of this genus are distributed across the water column of photic zone of the ocean with physiological and genetic correlation [13]. *Prochlorococcus* cells can absorb the blue light that penetrates the deep euphotic zone in the ocean [14], via Chl a_2 and Chl b_2. The presence of Chls a_2 and b_2

https://doi.org/10.1016/j.heliyon.2018.e01100

helps *Prochlorococcus* become the most abundant organisms in the deep euphotic zone [15].

The absorption spectrum of Chl b_2 shows a red shift and a high molar extinction coefficient (Ɛ) in the Soret band corresponding to the prevailing blue light that penetrates the deep ocean. The Q_y band (red band) of Chl b_2 has a higher energy level than Chl a_2; the energy transfer is from Chl b_2-rich regions to the adjacent Chl a_2. Furthermore, the fluorescence emission spectrum of Chl b_2 overlaps the absorption spectrum of Chl a_2 in acetone solution [16]. *Prochlorococcus marinus* MIT9313 (hereafter MIT9313) is a low-light adapted ecotype that is isolated from the Gulf Stream at 135 m below sea level [17]. Their genome size is 2.41×10^6 bp [18] with a diameter of <1 μm and its appearance in the planet was prior to the *Prochlorococcus* radiation [19, 20].

In the annotated genome of MIT9313 (GenBank: BX548175.1), the genes encoding phycobilisome structural proteins and enzymes involved in the phycocyanobilin biosynthesis are missing, although some of the genes involved in the phycoerythrin proteins remain. Interestingly, there is one copy of the 21 genes encoding for the PSII proteins; only *psb*A has two genes that encode identical D1 proteins. All PSI genes (11 genes) in MIT9313 are single-copy, and the 7 genes that encode the subunits of the cytochrome b_6f complex are also single-copy.

MIT9313 has two genes that encode chlorophylls *a/b*-binding proteins (Pcb): *pcb*A and *pcb*B [18, 21]. Pcb proteins are paralogs of the CP43 protein and belongs to CP43-like superfamily proteins [20, 22]. The Pcb proteins, constitute the light-harvesting antenna in MIT9313 [18]. PcbB (Mw 38.5×10^3 Dalton, kDa) is a constitutive antenna protein, but *pcb*A is expressed under stress by iron depletion (Mw 40.7 kDa). These proteins work as antenna in PSII and PSI, respectively [23]. Interestingly, the electron donor for PSI could be either plastocyanin (*pet*E) or cytochrome c_6 (*pet*J). Similarly, there are also three genes for PSI acceptors: two encoding ferredoxins (*pet*F1-2) and one-inducible gene for flavodoxin, *isi*B [23]. Finally, for the ferredoxin-$NADP^+$ oxidoreductase (FNR) gene, *pet*H, there is an N-terminal domain with a predicted transmembrane helix that could anchor FNR to the thylakoid membrane [24]. This contrasts with FNR from freshwater cyanobacteria whose N-terminal domain is similar to a phycocyanin-associated cap linker polypeptide, allowing specific binding of this protein to phycobilisomes [25, 26]. The prochlorophytes, like green algae and plants have a light-harvesting antenna integrated into the membrane; they also use chlorophyll *b* in their photosynthetic apparatus [21]. The structural arrangement of light-harvesting antennae of the PcbA with PSI forms an 18-mer ring around the PSI trimer [27]. In PSII, there are up to 8 molecules of the constitutive light-harvesting antenna protein, PcbB are associated with each PSII dimer. There are four PcbB antennae flanking each side of the PSII dimer [23, 27, 28]. In *Prochloron didemi,* the same structural pattern was observed, 10-Pcb

https://doi.org/10.1016/j.heliyon.2018.e01100

subunits are associated with the PSII dimer forming a giant complex with an estimated Mr of 1,500 kDa [27]. In *Prochlorothrix hollandica* contains *pcb*A, *pcb*B, and *pcb*C genes, and PcbC was coupled to PSI; PcbA and PcbB likely function as mobile antennae [29].

Cyanobacteria with PBS as the peripheral light-harvesting antenna have a core or proximal light-harvesting antenna of the PSs that contain Chl *a* as the harvesting pigment. In prochlorophyta, the green cyanobacteria have an integral membrane protein as the peripheral light-harvesting antenna. The core or proximal antenna of the PSs contains Chl *b* or b_2 in addition to Chl *a* or a_2 [27, 29, 30]. In contrast, plants that have a core antenna exclusively containing Chl *a* in the light harvesting complexes (LHC) variable Chl *b*/*a* ratios are present [31, 32].

The purpose of this study was to characterize the membrane complexes and the distribution of the pigments in the photosynthetic apparatus of *Prochlorococcus marinus* MIT9313. The membrane complexes were isolated by clear native electrophoresis (CN-PAGE) and sucrose gradient centrifugation. In both approaches, their protein components and pigments were identified by mass spectrometry. The PSII-PcbB supercomplexes and PSI trimers were identified. The cytochromes b_6f complex and ATP-synthase were also found. In sucrose gradient-enriched green fractions, the following Chl b_2/Chl a_2 molecular ratios were determined 2.16, 1.86, and 2.61 for Photosystem I, Photosystem II and PcbB, respectively. This abundance of Chl b_2 in photosynthetic apparatus (especially in PSI) has no precedent in organisms with oxygenic photosynthesis. Finally, the N-terminal domain of the FNR contains a sequence that predicts a transmembrane helix. Thus, this FNR could be a membrane-bound protein [24]. In this investigation, we established the presence of FNR in the thylakoid membranes from *Prochlorococcus marinus* MIT9313, probably bound to cytochrome b_6f complexes.

2. Materials and methods

2.1. Growth conditions and isolation of thylakoid membranes

MIT9313 was kindly provided by S. W. (Penny) Chisholm from MIT. Cells were grown in artificial seawater-based AMP1 medium, following the recommendations for large volumes (http://chisholmlab.mit.edu). Cultures (18 L) were bubbled with normal air under low intensities of white light (1.2 μmol photons m^{-2} s^{-1}) for 2 months. Cells were harvested and mixed with sea sand 1:3 (Merck). All subsequent steps were performed at 4 °C. Cells were ground for 3 min in a mortar and resuspended with 5 volumes of buffer containing 50 mM Bis-Tris pH 7.5, 100 mM NaCl, 1% sodium azide, and 1 mM phenylmethanesulfonyl fluoride (PMSF). The unbroken cells and sea sand were removed by centrifugation at 3,000 g for 15 min; this supernatant was then centrifuged at 126,000 g for 20 min. The thylakoids

https://doi.org/10.1016/j.heliyon.2018.e01100

in the pellet were resuspended in buffer containing 50 mM Bis-Tris pH 7.0, 500 mM aminocaproic acid, 2 mM $CaCl_2$, 10% glycerol, 1% sodium azide and 1 mM PMSF (sample buffer). The total divinyl chlorophylls (DV-Chls) concentration was adjusted to 1 mg mL^{-1}, and aliquots of 1−2 mL were rapidly frozen in liquid nitrogen and stored at −70 °C.

2.2. CN-PAGE and 2-D SDS-PAGE

CN-PAGE was performed as described in Wittig et al. [33]. Solubilization, centrifugation, and CN-PAGE were carried out at 4 °C. Thylakoids were quickly thawed and solubilized with 1% (w/v) of DDM for 30 min followed by centrifugation at 126,000 g for 20 min. The solubilized complexes were subjected to CN-PAGE in polyacrylamide gradient gels (4%−13% w/v) at 5 mA for 6 hours; the cathode buffer was supplemented with 0.01% DDM and 0.05% sodium deoxycholate (DOC). Some samples were loaded with double Chl concentration for second dimension sodium dodecyl sulfate polyacrylamide gel electrophoresis (2-D SDS-PAGE) followed by Coomassie brilliant blue staining or LC MALDI MS/MS. Lanes were cut out and incubated with 62.5 mM Tris-HCl pH 6.8, 20 mM dithiothreitol, 2.5% SDS and 10% glycerol for 2 h at 35 °C and subjected to 2-D SDS-PAGE in a 10% in a polyacrylamide gel.

Mitochondrial respiratory complexes (MRC) were used as molecular weight markers. To prepare MRC, 1 g of rat heart tissue was homogenized in 5 mL of sample buffer (without glycerol) with Polytron PT1300D (Fisher scientific, Hampton, NH, USA) at 2000 rpm for 1 min at 4 °C. Heart homogenate was centrifuged at 3,000 g for 10 min to remove tissue debris. Supernatant was aliquoted (200 μL) and centrifuged at 15,000 g for 20 min in a microfuge. The pellet was rapidly frozen in liquid nitrogen and stored at -70 °C. The pellet was resuspended in 50 μL of sample buffer and solubilized with 1% of DDM for 10 min and centrifuged at 126,000 g for 20 min [34]. The supernatant containing, MRC was subjected to CN-PAGE and 2-D SDS-PAGE under the same conditions used for the solubilized thylakoids of MIT9313.

2.3. RP-HPLC

Concentrated pigments were extracted from thylakoid membranes: 1 mg mL^{-1} of DV-Chl was vortexed with 6 mL of 90% methanol with 0.1 N of NH_4OH and incubated for 20 min at 60 °C in the dark. This extract was cooled on ice and centrifuged in a microfuge for 5 min. Aliquots (200 μL) of supernatant were injected and separated in a C-18 Kromasil column (AkzoNobel, Amsterdam, Netherlands; 4.6 × 250 mm, 5 μm particle size, 100 Å pore size) using a Dionex Ultimate 3000 HPLC-DAD with automatic injector and fraction collector (Thermo Scientific, Waltham, MA, USA). Pigments were separated according to Goerike, and Repeta [7] with minor

https://doi.org/10.1016/j.heliyon.2018.e01100

modification. Solvent A was methanol: 10 mM ammonium acetate (85:15), solvent B was 100% methanol, and solvent C was 100% acetone. The flow rate was 1.5 mL min^{-1} as follows: 0−5 min, 100% A; 5−12 min, 6% A, 92% B, 2% C; 12−15 min, 100% B; 15−18 min, 90% B, 10% C; 18−20 min, 40%B, 60%C; 20−24 min, 20% B, 80% C; 26−35 min, to equilibrate 100% A. Absorption spectra were recorded from 340 nm to 740 nm. Pigments with absorption at 450 nm were collected and protected from the light for further analysis.

2.4. ESI-MS/MS

Selected and collected peaks from RP-HPLC were directly injected into a Mass Spectrometer 3200 Qtrap with an ESI source (ABSciex, Framingham, MA, USA) at a rate of 10 μL min^{-1}. The compounds were analyzed in positive ion mode. All the MS spectra were generated using Enhanced MS (EMS) as the scan mode under the following parameters in the ionization source: Curtain Gas (CUR) = 10; Ion Spray Voltage (IS) = 5,500; Temperature (TEM) = 100 °C; Ion Source Gas 1 (GS1) = 10; Ion Source Gas 2 (GS2) = 0; Declustering Potential (DP) = 70; Entrance Potential (EP) = 10. All MS/MS spectra were generated by fragmentation of the precursor ion using high collision gas (CAD) and product ion as the scan mode. The ramp collision energy was set from 5 to 130 V for 3 min. The spectra obtained were interpreted to determine the structure of molecules. Carotenes-containing samples were supplied with 0.2% of trifluoroacetic acid (TFA) and 0.2% of hexafluorisopropanol (HFIP) to allow ionization.

2.5. Sucrose gradient centrifugation and divinyl chlorophyll determination

The solubilized thylakoids were loaded onto a 0.5−2 M linear sucrose gradient with a buffer containing 50 mM Bis-Tris pH 7.5, 100 mM NaCl, 1% sodium azide, 1 mM of PMSF and 0.01% of DDM (w/v). Tubes (18 mL total volume) were centrifuged at 260,000 g at 4 °C for 3 h. The gradients were collected bottom to top in 1 mL aliquots. Absorption spectra of all fractions (Fr) were obtained by scanning from 340 nm to 740 nm with a U-3310 spectrophotometer (Hitachi, Tokyo, Japan). Pigments were extracted from the sucrose gradient fractions using 80% acetone; the turbid samples were centrifuged at 15,000 g. Absorption spectra were recorded from 340 nm to 740 nm. DV-Chls concentrations were obtained by simultaneous equations [35] using extinction coefficients (ε, mM^{-1} cm^{-1}): for Chl b_2, ε_{654} 33.81 and ε_{664} 15.5; for Chl a_2 ε_{664} 69.29 and ε_{654} 34.93.

$$[\text{Chl } a_2] = [(2.18 * A_{664}) - (A_{654})] / 112.99$$

$$[\text{Chl } b_2] = [(1.98 * A_{654}) - (A_{664})] / 51.56$$

https://doi.org/10.1016/j.heliyon.2018.e01100

Five sucrose gradient experiments were used to determine DV-Chls concentrations. The average of 30, 20, and 25 measurements were used for fractions 3−8, 9−12, and 13−17, respectively; these were used to plot the [Chl b_2]/[Chl a_2] molecular ratios.

2.6. Assay for FNR activity

FNR diaphorase activity was measured by reduction of 2,6-dichlorophenolindophenol (DCPIP) with NADPH [26]. Reduction was followed for 1 min at 600 nm in all aliquots of sucrose fractions with a U-3310 spectrophotometer (Hitachi, Tokyo, Japan).

2.7. SDS-PAGE and immunoblot

SDS-PAGE and immunoblotting were performed as described [36], with minor modifications. The proteins in the gradient fractions were precipitated with 10% TCA final concentration and subjected to SDS-PAGE in a 14% polyacrylamide gel. The proteins in this gel were either stained with Coomassie brilliant blue or electrophoretically transferred to polyvinylidene fluoride (PDVF) membrane and subjected to immunodetection with rabbit antiFNR of *Arthrospira maxima* polyclonal antibodies. Goat anti-rabbit alkaline phosphatase conjugated antibodies were used to develop blots using nitro blue tetrazolium (NBT) and bromochloroindolyl phosphate (BCIP).

2.8. LC-MALDI-MS/MS

Twelve bands from a CN-PAGE were cut and enzymatically digested according to a modified protocol [37]. Resulting tryptic peptides were concentrated to ≅ 10 μL. Nine microliters were loaded into ChromXP Trap Column C18- CL pre-column (Eksigent, Redwood City, CA, USA; 350 μm × 0.5 mm, 120 Å pore size, 3 μm particle size) and desalted with 0.1% TFA in H_2O at flow of 5 μL min^{-1} for 10 min. The peptides were then loaded and separated on a Waters BEH130 C18 column (Waters, Milford, MA, USA; 75 μm × 150 mm, 130 Å pore size, 1.7 μm particle size) using a HPLC Ekspert nanoLC 425 (Eksigent, Redwood City, CA, USA) with a mobile phase A, 0.1% TFA in H_2O and mobile phase B 0.1% TFA in ACN under the following linear gradient: 0−3 min 10% B (90% A), 35 min 60% B (40% A), 36−45 min 90 % B (10% A), and 46−120 min 10% B (90% A) at a flow of 300 nL min^{-1}. The eluted fractions were automatically mixed with a solution of 2 mg/mL of alpha-cyano-4- hydroxycinnamic acid (Sigma-Aldrich, St. Louis, MO, USA) in 0.1% TFA and 50% ACN as the matrix. This was then spotted on an Opti-TOF plate with 384 spots using a MALDI Ekspot (Eksigent, Redwood City, CA, USA) with a spotting velocity of 30 s per spot with matrix flow at 1.6 μL min^{-1}. The spots were then analyzed by a MALDI-TOF/TOF 4800 Plus, mass spectrometer (ABSciex, Framingham, MA, USA). Each MS spectrum was acquired by an accumulating 1,000 shots in a mass range of 850−4,000 Da with a laser intensity

https://doi.org/10.1016/j.heliyon.2018.e01100

of 3,100. The 100 more intense ions with a minimum signal-noise (S/N) of 20 were programmed to fragmenting. The MS/MS spectra were obtained by fragmentation of the selected precursor ions using Collision Induced Dissociation (CID) and acquired by 3,000 shots with a laser intensity of 3,800. The resulting MS/MS spectra were compared using Protein Pilot software v.2.0.1 (ABSciex, Framingham, MA, USA) against the *Prochlorococcus* MIT9313 database (accession BX548175.1) using Paragon algorithm. Search parameters included carbamidomethylated cysteine, trypsin, all the biological modifications, amino acids substitution as set by the algorithm; a phosphorylation emphasis and Gelbased ID were special factors. The detection threshold was 2 to acquire 99% of confidence; also, the identified proteins observed a local FDR of 5% or less. The identified proteins were grouped by ProGroup algorithm in the software to minimize redundancy.

3. Results

3.1. Complexes and supercomplexes of thylakoid membranes from *Prochlorococcus marinus* MIT9313 solubilized with dodecyl maltoside and separated by two-dimensional electrophoresis

The photosynthetic apparatus in MIT9313 is organized in two supercomplexes in complete media: a naked PSI-trimer and a PSII-dimer surrounded by 8 light-harvesting subunits (PcbB). The peripheral antennae in the photosynthetic membranes are of two types: associated with the photosystems (fixed antenna) forming supercomplexes or as mobile antenna subjected to light regulation. Under iron depletion, the photosynthetic membranes of MIT9313 have PSI trimers that are surrounded by 18 light-harvesting proteins of PcbA [23]. PSII is a supercomplex formed by a dimeric PSII with up to 8 light-harvesting proteins (PcbB) in both media [23]. We used CN-PAGE to detect and to estimate the quantity of the supercomplexes of the photosynthetic apparatus. The supercomplexes can be extracted and isolated from the photosynthetic membrane and dissociate during the solubilization with detergent and during the centrifugation that precedes the electrophoresis. The dissociation and diffusion of the subunits of the complexes is limited in the gel, and we explored the distribution of the photosynthetic complexes. We obtained 80% of the DV-Chls bound to the proteins (Fig. 1a and b green and blue bands 1−10) and approximately 50% of them, were bound to the PSI and PSII supercomplexes, (green bands 1−3). The others were associated with the light-harvesting antenna oligomers (Fig. 1a). The more abundant components in the thylakoid membrane of MIT9313 are the proteins of the photosynthetic apparatus as seen in the gels stained with Coomassie blue (Fig. 1b and c). The apparent mass of the supercomplexes in the PSI trimers is 980 kDa (calculated 1,080 kDa). For PSII, they were 1,045, 980, and 829 kDa. The calculated mass for PSII dimers with 8 PcbB light-harvesting antennae was 1,196 kDa.

https://doi.org/10.1016/j.heliyon.2018.e01100

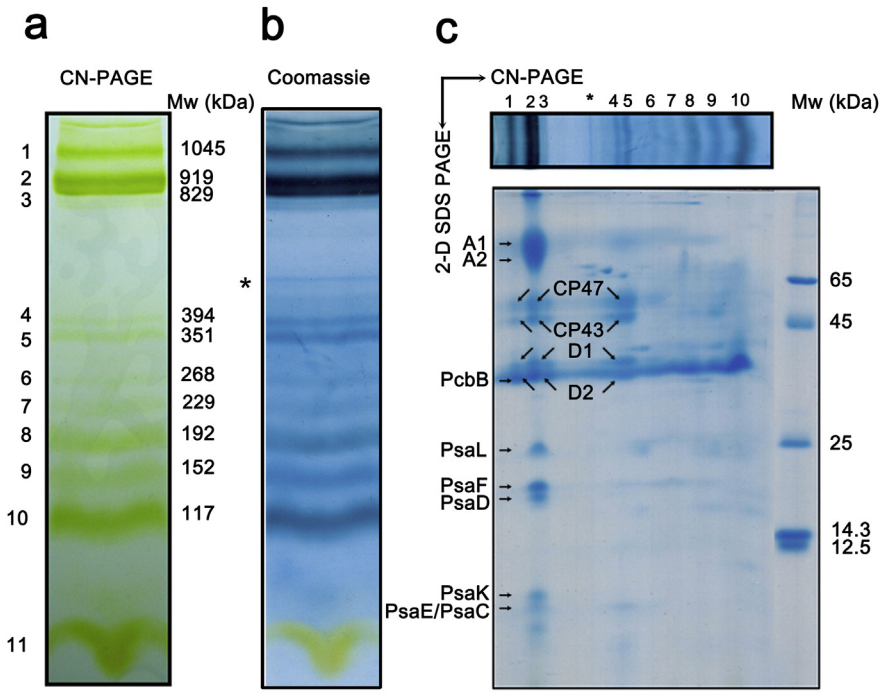

Fig. 1. Electrophoretic characterization of the photosynthetic apparatus of thylakoid complexes and supercomplexes from *Prochlorococcus marinus* MIT9313. a. CN-PAGE electrophoretogram of solubilized thylakoids from MIT9313 with 1% DDM. Green bands were numbered (1−11) at the left margin. Apparent masses are at the right side. b. Coomassie-blue staining of the CN-PAGE gel are shown in a, and an extra non-green band appeared (*). c. 2-D SDS-PAGE of CN-PAGE. A lane from the first dimension gel was cut, soaked in electrophoresis sample buffer, and applied to the second-dimension denaturing electrophoresis. An image of a stained CN gel is shown at the top. PSI subunits positions are shown at the left whereas PSII core subunits are inside the gel. Numbers at the right side of the gel are the masses of molecular markers: albumin (65 kDa), ovoalbumin (45 kDa), quimotripsynogen (25 kDa), lysozyme (14.3 kDa), and horse heart cytochrome *c* (12.5 kDa). Full, non-adjusted gels are available in Suppl. Fig. 1.

Chlorophyll/protein complexes of MIT9313 grown at 1.2 μmole photons s^{-1} m^{-2} of light intensity were solubilized with 1% of DDM and resolved into eleven green bands (Fig. 1a) in a polyacrylamide gradient gel after clear native electrophoresis (CN-PAGE). These bands (marked 1−11) were subjected to: a) a molecular weight analysis, b) a second dimension SDS-PAGE analysis (2-D SDS-PAGE), and c) mass spectrometry. To estimate the masses of the green protein bands in CN-PAGE, we used MRC as molecular weight markers [34]. In Suppl. Fig. 1b we compare the migration of complexes obtained from MIT9313 membranes with MRC and with high molecular weight water soluble proteins. To identify the MRC, we performed 2-D SDS-PAGE (Suppl. Fig. 1c).

The molecular weight markers were plotted in a semi-log plot of MRC versus their migration distance. We could interpolate the migration distance of the green bands and assigned the apparent masses. The apparent molecular masses of 10 of the green

https://doi.org/10.1016/j.heliyon.2018.e01100

bands are shown in the column of Mw (kDa) in Fig. 1a in a range of 117 to 1,045 kDa. Band 11 (green-brown color) is a mixture of free pigments (DV-Chls and carotenoids) in detergent micelles. The more intense green bands were: band 1 of 1,045 kDa, band 2−3 of 919−829 kDa, and band 10 of 117 kDa. These three bands together with bands of 394, 351, 192 and 152 kDa also appeared as intense bands in the Coomassie blue-stained gel (Fig. 1b). To assign the identity of green bands to the photosynthetic apparatus complexes, we calculated theoretical masses of the PSII monomer (21 protein subunits, including 36 Chls, and 13 carotenes pigments). This was 392 kDa.

The mass of the PSI monomer (11 protein subunits, including 96 Chls and 22 carotenoids) resulted in a mass of 360 kDa. The estimated mass for PcbB antenna subunit (including 13 Chl a_2 or Chl b_2) was 50 kDa. A 2-D SDS-PAGE was performed (Fig. 1c) with one lane to further characterize the green complexes separated by CN-PAGE. Another lane was subjected to mass spectrometry analysis (Tables 1, 2, 3, and 4). The green band 1 had an apparent molecular mass of 1,045 kDa. This was resolved on the second dimension into four intense Coomassie blue spots

Table 1. Proteomic identification of components of the photosynthetic apparatus from CN-PAGE bands 1−5 (Fig. 1a).

Band[a]	Uniprot ID	Total coverage	> 95% coverage	Gene[b]	Predicted mass (kDa)[c]	Subunit[d]
1	Q7TTH6	57.8	18.1	*psbA*	39.41	PSII-D1
	Q7V5A7	70.1	27	*psbB*	56.16	PSII-CP47
	Q7V6H9	68.8	17.8	*psbC*	50.9	PSII-CP43
	Q7V6I0	61.2	18.8	*psbD*	39.32	PSII-D2
	Q7V4Q1	69.3	44.8	*psbF*	5.44	PSII- Cyt b_{559}
	Q7V4P9	73.8	24.6	*psbJ*	6.88	PSII-PsbJ
	Q7V6U4	59.1	27.4	*pcbB*	38.54	Antenna-PcbB
	Q7V512	60.9	16.5	*psaL*	20.07	PSI-XI
2 and 3	Q7TTH6	65	11.7	*psbA*	39.41	PSII-D1
	Q7V5A7	64.3	22.9	*psbB*	56.16	PSII-CP47
	Q7V6H9	55.9	14.4	*psbC*	50.9	PSII-CP43
	Q7V6I0	35.8	3.7	*psbD*	39.32	PSII-D2
	Q7V6U4	42	9.7	*pcbB*	38.54	Antenna-PcbB
	Q7V8Y4	97	67.6	*psaE*	7.64	PSI-IV
	Q7V510	46	3.7	*psaA*	84.98	PSI-A1
	Q7V511	33.7	4.5	*psaB*	83.23	PSI-A2
	Q7V564	66.1	21.1	*psaD*	15.75	PSI-PsaD
	Q7V659	62.9	17.6	*psaF*	18.43	PSI-III
	Q7V7Q1	59.3	18.6	*psaK*	8.99	PSI-X
	Q7V512	35.2	16.5	*psaL*	20.07	PSI-XI
4 and 5	Q7TTH6	37.7	14.5	*psbA*	84.98	PSII-D1
	Q7V5A7	23.7	20.9	*psbB*	56.16	PSII-CP47
	Q7V6H9	20.2	9.2	*psbC*	50.90	PSII-CP43

[a] Apparent masses of bands: 1, 1046 kDa; 2, 920 kDa; 3, 830 kDa; 4, 394 kDa; 5, 351 kDa.
[b] Data obtained from MIT 9313 genome BX548175.1. used by mass spectrometry software.
[c] Predicted mass of the gene product.
[d] Protein subunit from PDB 1JB0 for PSI, from 3WU2 for PSII.

https://doi.org/10.1016/j.heliyon.2018.e01100

Table 2. Proteomic identification of components of CN-PAGE band 6 and 7 (Fig. 1a).

Band[a]	Uniprot ID	Total coverage	> 95% coverage	Gene[b]	Predicted mass (kDa)[c]	Function[d]
6	Q7V5A7	79.8	24.9	*psbB*	56.16	PSII-CP47
	Q7TTH6	64.5	14.5	*psbA*	39.41	PSII-D1
	Q7V6I0	69.8	9.1	*psbD*	39.32	PSII-D2
	Q7V6U4	73.1	17.1	*pcbB*	38.54	Antenna-PcbB
	Q7V653	69.3	8.3	*petA*	33.33	Cyt *f*
7	Q7TTH6	70.6	15.3	*psbA*	39.41	PSII-D1
	Q7V5A7	59	12.3	*psbB*	56.16	PSII-CP47
	Q7V6H9	63	6.2	*psbC*	50.90	PSII-CP43
	Q7V6I0	37.3	3.7	*psbD*	39.32	PSII-D2
	Q7V6U4	44.2	14.5	*pcbB*	38.54	Antenna-PcbB
	Q7TUW1	65.8	7.9	*petH*	40.89	FNR
	Q7V654	34.8	8.4	*petC*	18.86	Rieske protein

[a] Apparent masses of bands: 6, 268 kDa; 7, 230 kDa.
[b, c] Parameters as in Table 1.
[d] Protein subunit from PDB 1VF5 for cytochrome b_6f complex.

Table 3. Proteomic identification of components from CN-PAGE band 8 (Fig. 1a).

Uniprot ID	Total coverage	> 95% coverage	Gene[b]	Predicted mass (kDa)[c]	Subunit[d]
Q7V4Q0	41	41	*psbL*	4.46	PSII-PsbL
Q7V6H9	38.7	31.3	*psbC*	50.90	PSII-CP43
Q7V5A7	41.9	25.4	*psbB*	56.16	PSII-CP47
Q7V4P9	43	24.6	*psbJ*	6.88	PSII-PsbJ
Q7V6I0	25	18.8	*psbD*	39.32	PSII-D2
Q7V4Y4	27.9	12.5	*psbO*	29.06	PSII-PsbO
Q7TUU3	19.1	6.1	*psb27*	16.19	PSII-Psb27
Q7V6U4	58.2	43.1	*pcbB*	38.54	Antenna-PcbB
Q7V511	22.4	8.5	*psaB*	83.23	PSI-A2
Q7TTH6	26.2	5.3	*psaA*	84.98	PSI-A1
Q7V653	28	22.9	*petA*	33.33	Cyt *f*
Q7V5B9	25.2	9.6	*petB*	24.57	Cyt b_6
Q7TUW1	50	9	*petH*	40.89	FNR
Q7V5S4	33.1	9.2	*atpG*	16.72	b' subunit Fo
Q7V5S5	63.3	6.9	*atpF*	18.72	b subunit Fo
Q7V5S7	23.7	5.7	*atpA*	54.04	α subunit F_1
Q7V5S8	33.8	5.6	*atpC*	35	γ subunit F_1
Q7V5U2	35	2.8	*atpD*	52.13	β subunit F_1

Apparent mass of band 8, 192 kDa.
[b, c] Parameters as in Table 1.
[d] Protein subunits from PDB 5DN6 for ATP synthase.

https://doi.org/10.1016/j.heliyon.2018.e01100

Table 4. Proteomic identification of components from CN-PAGE bands 9 and 10 (Fig. 1a).

Band[a]	Uniprot ID	Total coverage	> 95% coverage	Gene[b]	Predicted mass (kDa)[c]	Subunit[d]
9	Q7TV66	74.1	45	*psbU*	13.10	PSII-PsbU
	Q7V4Q0	76.9	41	*psbL*	4.46	PSII-PsbL
	Q7V5A7	49.8	31.1	*psbB*	56.16	PSII-CP47
	Q7V6H9	52	30.9	*psbC*	50.90	PSII-CP43
	Q7V4P9	73.8	24.6	*psbJ*	6.88	PSII-PsbJ
	Q7V6I0	46.1	16.8	*psbD*	39.32	PSII-D2
	Q7V4Q1	73.4	16.3	*psbF*	5.44	PSII-Cyt b_{559}
	Q7V6U4	50.2	34	*pcbB*	38.54	Antenna-PcbB
	Q7V512	32	16.5	*psaL*	20.07	PSI-XI
	Q7TTH6	33.5	11.7	*psaA*	84.98	PSI-A1
	Q7V511	26.4	6.2	*psaB*	83.23	PSI-A2
	Q7V9A0	69.5	5.3	PMT_0054	20.52	Putative Ycf37
	Q7V653	83.8	58.3	*petA*	38.54	Cyt f
	Q7V5B9	39.4	15.5	*petB*	24.74	Cyt b_6
	Q7V654	29.2	8.4	*petC*	18.86	Rieske protein
	Q7TUW1	40.1	4.	*petH*	40.89	FNR
	Q7V5U2	74.1	40.9	*atpD*	52.13	β subunit F_1
	Q7V5S7	54.2	16	*atpA*	54.04	α subunit F_1
	Q7V5S2	53.5	12.4	*atpB*	27.17	a subunit Fo
	Q7V5S6	63.1	8.2	*atpH*	19.70	δ subunit F_1
	Q7V5S5	70.3	6.9	*atpF*	18.72	b subunit Fo
	Q7V590	56.1	10.9	*cpeA*	16.97	α Phycoerythrin
10	Q7V6H9	47.7	6.2	*psbC*	50.90	PSII-CP43
	Q7V6U4	55.1	33.7	*pcbB*	38.54	Antenna-PcbB
	Q7V5U2	57.5	18.2	*atpD*	52.13	β subunit F_1
	Q7V5S7	64.7	5.7	*atpA*	54.04	α subunit F_1

[a] Apparent masses of bands: 9, 152 kDa; 10, 117 kDa.
[b, c, d] Parameters as in Table 1.

at 54, 49, 38, and 35 kDa corresponding to CP47, CP43, D1, D2, and antenna protein (PcbB), respectively; all of these subunits are PSII.

Other components of PSII also identified by mass spectrometry in the green band 1 were PsbF and PsbJ (Table 1). The predicted molecular mass of the supercomplex formed by a PSII dimer and eight PcbB antenna subunits, (as the one described by Bibby et al. [23], resulted in a mass of 1,180 kDa, close to the apparent mass obtained in CN-PAGE for the green band 1 (1,045 kDa, Fig. 1a). The split-green band 2 has an apparent mass of 919 kDa (Fig. 1a). This was resolved in 11 Coomassie blue spots on the 2-D SDS-PAGE with apparent masses of 80−71, 56, 51, 39, 36, 23, 18, 17, 9.7, 9, and 8 kDa (Fig. 1c). These are subunits of PSII and PSI and represent the same components referred above for PSII (underlined). The others are subunits of PSI: A1, A2, IX, III, II, IV, and X subunits. The subunits of both PSs were identified by mass spectrometry (Table 2). The calculated mass for the PSI trimer for MIT9313, was 1,080 kDa.

In conclusion, the split-green band 2 is the co-migration of PSI trimer and a supercomplex of PSII dimer with 4 PcbB subunits. Green band 3 has an apparent mass of

https://doi.org/10.1016/j.heliyon.2018.e01100

829 kDa and had the core subunits of PSII in the 2D analysis of the CN-PAGE (Fig. 1c). Green bands 4 and 5 with light green color have apparent masses of 394 and 351 kDa and were intensely stained with Coomassie blue (Fig. 1b). In the 2-D SDS-PAGE analysis, the more intense spots corresponded to the core subunits of PSII: CP47, CP43, D1, and D2. When we calculated the stoichiometry of subunits with software Image lab (BioRad), we obtained one subunit of each. This result was corroborated by mass spectrometry; no antenna subunits (PcbB) appeared here (Table 3). The calculated molecular mass of the PSII monomer for MIT9313 was 398 kDa, which agrees with the apparent mass of 351−394 kDa obtained in the CN-PAGE in Fig. 1a. Light Coomassie blue spots of PSI also appeared. The calculated molecular mass of PSI monomer (360 kDa) is in the range of the apparent mass obtained in the CN-PAGE. The green bands 6−10 with molecular masses of 268 kDa, 229 kDa, 192 kDa, 152 kDa, and 117 kDa respectively, were assigned as antenna oligomers of PcbB. This appeared as an intense Coomassie blue line at 35−37 kDa in the 2-D SDS-PAGE (Fig. 1c). The presence of oligomers may be a consequence of the detergent solubilization procedure that affects the supramolecular structure of the thylakoid membrane complexes.

3.2. Proteomic identification of the complexes and supercomplexes in CN-PAGE by mass spectrometry

Bands 6 to 10 in CN-PAGE (Fig. 1a) were subjected to mass spectrometry analysis (Tables 1, 2, 3, and 4). In band 6 (268 kDa), the proteins identified were: the core of PSII; and the cytochrome *f* from the cytochrome b_6f complex (Table 3). Band 7 (229 kDa) substructures of PSII contain the RC proteins D1 and D2, the core antenna, CP43, and CP47. FNR and the iron-sulfur subunit (Rieske) of the cytochrome b_6f complex were also detected (Table 2). Band 8 (192 kDa) has proteins that correspond to the four membrane complexes of the oxygenic photosynthesis (Table 3). PSII has the core proteins, CP43, CP47 and D2; the β-barrel subunit PsbO, an important protein for the stabilization of the oxygen evolving complex; and the peripheral subunits, PsbJ and PsbL. It also had the luminal subunit Psb27 which is involved in the repair and assembly of PSII [38, 39]. This has a role as a gate-keeper Mn-cluster assembly [40].

The RC subunits A1 and A2 were identified for PSI. For ATP synthase, subunits of the F_1 substructure, α, β, and γ subunits, and from F_0 subunits, b' and b were identified. For the cytochrome b_6f complex, b_6 (PetB) and *f* (PetA) were identified, and peptides from FNR (PetH) were identified with the best confidence values at this band (Table 3). In band 9, (152 kDa) the proteins also correspond to the four membrane complexes of the oxygenic photosynthesis (Table 4). For PSII, the core proteins CP43, CP47, D1, and D2, were detected along with the luminal subunit, PsbU and one subunit of the cytochrome b_{559} (PsbF). For PSI, the RC subunits

https://doi.org/10.1016/j.heliyon.2018.e01100

A1 and A2 as well as the peripheral subunit PsaL and a putative protein Ycf37. This protein has been suggested to be involved in stability and assembly of PSI [41] as well as in the biogenesis and preservation of the PSI trimer [42]. For the cytochrome b_6f complex, the three active components cytochromes b_6, cytochrome *f,* and the iron-sulfur protein (Rieske) were observed with the best confidence values. The FNR was identified at this band too. For ATP synthase, other subunits were detected at this band. The α, β, and δ were seen for the F_1 substructure and a and b were seen in the F_0 substructure. Band 10 was the richest band in light-harvesting protein PcbB. The light-harvesting subunit PcbB was confirmed in all bands (except bands 4 and 5). Other proteins include CP43 from PSII and α and β from the F_1 substructure of ATP synthase. Other membrane proteins were detected by mass spectrometry in the green bands (Suppl. Table Raw material).

3.3. Identification of the membrane complexes obtained in the sucrose gradient centrifugation by SDS-PAGE and mass spectrometry

Chl-binding protein complexes of MIT9313 were resolved in three main bands in a sucrose density gradient after centrifugation of thylakoid membranes solubilized with DDM. The sucrose gradient was collected in 18 fractions (Fr) of 1 mL, from bottom to top. The Fr were subjected to spectrophotometric analysis and measurement of diaphorase activity. Fig. 2a shows the sedimentation profile of a sucrose gradient. The absorption profiles at 681 nm for Chl a_2 and 651 nm for Chl b_2

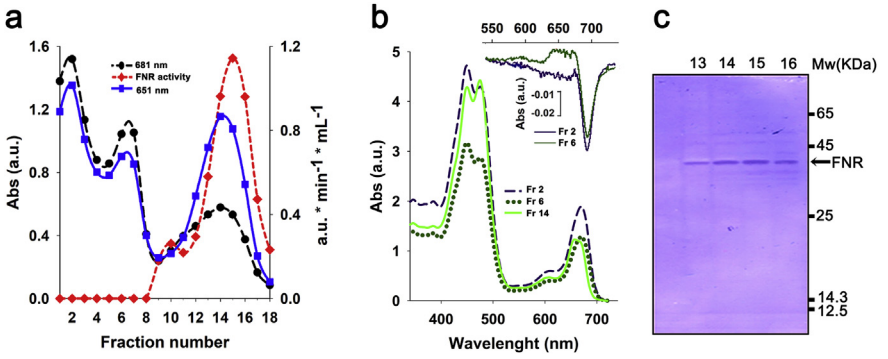

Fig. 2. Characterization of fractions obtained by sucrose gradient centrifugation of solubilized thylakoids from *Prochlorococcus marinus* MIT9313. a. Patterns of fractions obtained by sucrose gradient centrifugation. Thylakoids were solubilized with DDM (1% w/w) and loaded onto the sucrose gradient and collected 1 mL per fraction (bottom to top). Visible absorption spectrum of each fraction was recorded. Absorption (left axis) at wavelengths at 681 nm and 651 nm were chosen to show the distribution of Chl a_2 (circles) and b_2(squares) in the fractions of the sucrose gradient. Diaphorase activity (ordinate axis, at right) was measured in all fractions of the sucrose gradient (diamonds). b Absorption spectra of fractions 2, 6 and 14 (from a) are shown. Insert Photobleaching of P_{700} were detected in fraction 2 (Fr 2) and fraction 6 (Fr 6). c Immunoblot of fractions 13−16 probed with FNR-antibody. Proteins of the fractions of sucrose gradient were separated by SDS-PAGE. The immunoblot used an anti-*A. maxima* FNR antibody. Full, non-adjusted blot is available in Suppl. Fig. 2.

https://doi.org/10.1016/j.heliyon.2018.e01100

show three peaks centered at Fr 2, 6, and 14. The 651 nm/681 nm absorption ratio of the fast (Fr 2) and medium bands (Fr 6) are close to 1 but the slow band (Fr 14) has a ratio of 2. The absorbance spectra of Fr 2, 6, and 14 are shown in Fig. 2b. The ratio Soret band/red band is higher for the spectrum of Fr 14 (continuous line) than in Fr 2 and Fr 6, indicating that Fr 14 was most enriched in Chl b_2.

The insert in Fig. 2b has the corrected spectra of oxidized P_{700} (by white actinic light) minus reduced (by ascorbate) of Fr 2 and Fr 6. This shows the presence of PSI in both bands.

In the sucrose gradient, PSI trimers (Fig. 2a Fr 2) and monomers (Fig. 2a Fr 6), antenna oligomers (Fig. 2a Fr 13−17), and FNR (Fig. 2c Fr 13−16) were detected. However, we did not obtain evidence of the presence of PSII. Looking for PSII proteins, all 16 sucrose gradient fractions in Fig. 3a were analyzed by SDS-PAGE (Fig. 3b). This analysis revealed several bands: in Fr 1−7 at apparent molecular masses of 70−75 kDa identified as A1 and A2 core subunits of PSI, the bands at 15−20 kDa correspond to PsaD (subunit II), PsaF (subunit III) and PsaL (subunit XI). The more intense bands were in Fr 2 and Fr 6 (left arrowheads), the peaks of trimers and monomers of PSI, respectively (Fig. 3a). The bands that correspond to PSII proteins are seen in Fr 9−11 at 45−47 kDa, (CP47 and CP43) and at 35−39 kDa corresponding to D1 and D2 of the RC of PSII. The presence of the PSII in Fr 9−11 was observed in *Leptolyngbya* CCM4 [43].

To complete the analysis of the sucrose gradient, the gel bands of Fig. 3b marked with an asterisk (*) were cut and processed for mass spectrometry. The results

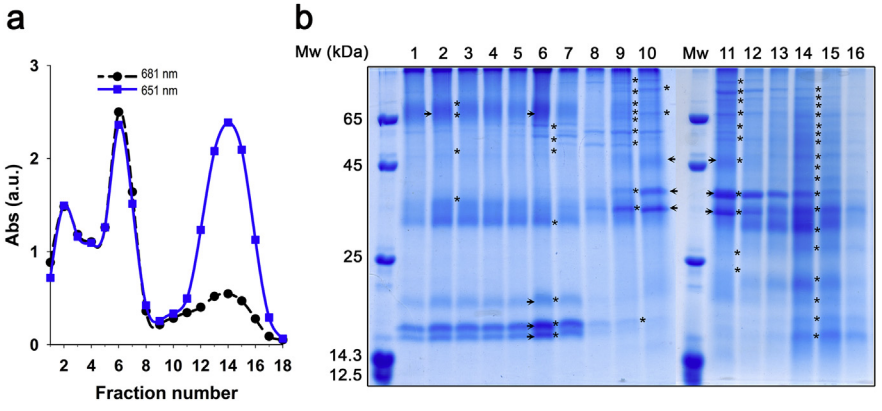

Fig. 3. SDS-PAGE analysis of fractions of the sucrose gradient. a. Chlorophyll light absorption of fractions (bottom to top) obtained from sucrose gradient centrifugation. Absorption parameters are as in Fig. 2a. b. Coomassie blue stained gel of sucrose gradient fractions. The protein concentration of each fraction was estimated, and approximately 50 μg of protein was precipitated with cold TCA. Precipitates were suspended in 25 μL of digestion buffer and were loaded in the gel. Bands with an asterisk (*) were excised and subjected to ESI MS/MS analyses. The proteins of the photosynthetic apparatus, F_0F_1 ATP synthase and b_6f complex identified are in Tables 5, 6, and 7. Full, non-adjusted gels are available in Suppl. Fig. 3.

https://doi.org/10.1016/j.heliyon.2018.e01100

can be seen in Tables 5, 6, and 7. In Table 5 up to 5 subunits of PSI were identified corroborating the core subunits A1 and A2 and the medium size subunits XI, II and III as expected in Fr 2 and Fr 6. They were also detected in Fr 9 and Fr 10 as traces via with the Coomassie intensity in the electrophoretogram. Traces of the four characteristic PSII proteins D1, D2, CP43, and CP47 were detected by mass spectrometry (Table 6) in the region of the high molecular weight complexes in Fr 2 and Fr 6. However, according to the intensity of the Coomassie blue stain, they were more abundant in Fr 9−11 (arrows between Fr 10 and Fr 11 of Fig. 3b). The conspicuous bands of the core components of PSII in Fr 9−11 were confirmed by mass spectrometry in Table 6. The great abundance of antenna protein PcbB can be seen as an intense band with an apparent mass of 35 kDa. In the DV-Chls profile of Fig. 3a, we can see that the peak of Chl b_2 is in Fr 14. Also, in mass spectrometry analysis, PcbB was the most common protein in all the fractions especially in Fr 14. Only traces of the ATP synthase in different fractions were observed similar to CN-PAGE, analysis. This is probably as a consequence of the detergent solubilization procedure used, which could affect the supramolecular structure of this enzyme.

Table 5. Proteomic identification of PSI subunits in the sucrose gradient fractions (Fig. 3a). Analysis of the fractions by SDS-PAGE (Fig. 3b*).

Fraction No.[a]	Uniprot ID	Gene[b]	Predicted mass (KDa)[c]	Times detected[d]	Pp unique[e]	Coverage (%)	Subunit[f]
2	Q7V659	*psa*A	84.9	4	9	12	PSI-A1
	Q7V511	*psa*B	83.2	3	11	14.7	PSI-A2
	Q7V564	*psa*D	15.7	4	5	43	PSI-II
	Q7V511	*psa*F	18.4	2	3	21	PSI-III
	Q7V511	*psa*L	20.1	2	4	26	PSI-XI
6	Q7V659	*psa*A	84.9	5	8	10.8	PSI-A1
	Q7V511	*psa*B	83.2	5	11	14.6	PSI-A2
	Q7V564	*psa*D	15.7	6	28	90	PSI-II
	Q7V511	*psa*F	18.4	4	10	51	PSI-III
	Q7V511	*psa*L	20.1	6	23	52	PSI-XI
	Q7V6I1	PMT_1178	20.7	1	3	20.9	Putative Ycf4
9	Q7V659	*psa*A	84.9	6	11	13.9	PSI-A1
	Q7V511	*psa*B	83.2	7	13	17.5	PSI-A2
	Q7V564	*psa*D	15.7	5	10	57	PSI-II
	Q7V511	*psa*F	18.4	2	21	53	PSI-III
	Q7V511	*psa*L	20.1	5	3	15	PSI-XI
10	Q7V659	*psa*A	84.9	1	8	10.6	PSI-A1
	Q7V511	*psa*B	83.2	2	7	10.3	PSI-A2
	Q7V564	*psa*D	15.7	1	3	26	PSI-II
	Q7V511	*psa*L	20.1	1	3	21	PSI-XI
11	Q7V511	*psa*B	83.2	2	5	9.7	PS-I-A2
	Q7V9A0	PMT_0054	20.5	1	3	22	Putative Ycf37

[a] Sucrose gradient fraction. Bands were cut from SDS-PAGE shown in Fig. 3b * and analyzed by mass spectrometry.
[b, c, f] Parameters as in Table 1.
[d] Number of times that the protein was identified in the mass spectra, in different bands of the same fraction lane in the gel.
[e] Number of unique peptide of the protein with >95% probability of identity.

https://doi.org/10.1016/j.heliyon.2018.e01100

Table 6. Proteomic identification of PSII subunits in the sucrose gradient fractions separated (Fig. 3a). Analysis of the fractions by SDS-PAGE (Fig. 3b*).

Fraction No.[a]	Uniprot ID	Gene[b]	Predicted mass (kDa)[c]	Times detected[d]	Pp unique[e]	Coverage (%)	Subunit[f]
2	Q7V5B9	*psb*B	56.16	2	9	21	PSII-CP47
	Q7V6H9	*psb*C	50.9	3	6	13	PSII-CP43
	Q7V6I0	*psb*D	39.32	3	3	9	PSII-D2
	Q7V6U4	*pcb*B	38.54	4	12	25	Antenna-PcbB
6	Q7V5B9	*psb*B	56.16	5	15	33	PSII-CP47
	Q7V6H9	*psb*C	50.9	3	5	13	PSII-CP43
	Q7V6I0	*psb*D	39.32	4	4	14	PSII-D2
	Q7V6U4	*pcb*B	38.54	9	12	29	Antenna-PcbB
9	Q7TTH6	*psb*A	39.41	5	4	15	PSII-D1
	Q7V5B9	*psb*B	56.16	9	25	38	PSII-CP47
	Q7V6H9	*psb*C	50.9	6	6	15	PSII-CP43
	Q7V6I0	*psb*D	39.32	9	5	20	PSII-D2
	Q7V6U4	*pcb*B	38.54	7	11	29	Antenna-PcbB
10	Q7TTH6	*psb*A	39.41	1	5	18.4	PSII-D1
	Q7V5B9	*psb*B	56.16	2	24	36.7	PSII-CP47
	Q7V6H9	*psb*C	50.9	2	5	11.4	PSII-CP43
	Q7V6I0	*psb*D	39.32	2	8	23.4	PSII-D2
	Q7V6U4	*pcb*B	38.54	2	8	15.4	Antenna-PcbB
11	Q7TTH6	*psb*A	39.41	4	5	18.4	PSII-D1
	Q7V5B9	*psb*B	56.16	11	21	39.0	PSII-CP47
	Q7V6H9	*psb*C	50.9	6	4	11.4	PSII-CP43
	Q7V6I0	*psb*D	39.32	8	6	19.1	PSII-D2
	Q7V6U4	*pcb*B	38.54	9	10	28	Antenna-PcbB
14	Q7TTH6	*psb*A	39.41	3	4	12.3	PSII-D1
	Q7V5B9	*psb*B	56.16	12	8	14.7	PSII-CP47
	Q7V6H9	*psb*C	50.9	13	8	15.1	PSII-CP43
	Q7V6I0	*psb*D	39.32	10	4	9.7	PSII-D2
	Q7V6U4	*pcb*B	38.54	17	16	27.1	Antenna-PcbB

[a, b, c, d, e, f] Parameters as in Table 5.

3.4. The presence of ferredoxin NADP$^+$ reductase in the thylakoid membranes

As indicated above, in bands 7−9 of CN-PAGE, peptides from FNR (PetH) were identified with best confidence values at band 8 (Table 3). In these bands, the following components of cytochrome b_6f complex, b_6 (PetB), f (PetA) and Rieske protein (PetC) were also identified (Tables 2, 3, and 4). We analyzed *in silico* the amino acid sequence N-terminal of FNR from *Prochlorococcus* MED4 [24], which has a segment that predicts a transmembrane helix (Suppl. Fig. 2b). This predicted transmembrane helix was found in 9 more species of *Prochlorococcus* (Suppl.

https://doi.org/10.1016/j.heliyon.2018.e01100

Table 7. Proteomic identification of cytochrome b_6f, FNR and F_1F_0 ATP synthase subunits in the sucrose gradient fractions (Fig. 3a). Analysis of the fractions by SDS-PAGE (Fig. 3b *).

Fraction No.[a]	Uniprot ID	Gene[b]	Predicted mass (kDa)[c]	Times detected[d]	Pp unique[e]	Coverage (%)	Subunit[f]
14	Q7V653	*petA*	33.3	2	4	22.9	Cyt *f*
	Q7V5B9	*petB*	24.5	3	4	27	Cyt b_6
	Q7TUW1	*petH*	40.8	5	6	20	FNR
14	Q7V5S7	*atpA*	54.0	1	3	7.3	α subunit F_1
	Q7V5U2	*atpD*	52.1	1	4	9.2	β subunit F_1
	Q7V5S5	*atpF*	18.7	1	6	37	b subunit Fo
	Q7V5S6	*atpH*	19.7	1	5	24	δ subunit F_1

[a, b, c, d, e, f] Parameters as in Table 5.

Fig. 2c). In agreement with this, both a Coomassie blue-stained band (identified as FNR by apparent molecular mass in Suppl. Fig 2d) in thylakoid membranes, and a band immunodected with anti-*A. maxima*-FNR antibodies, presented an expected molecular mass of 40 kDa (Suppl. Fig 2e).

In DDM-solubilized protein complexes from thylakoid membranes separated in a sucrose gradient, the diaphorase enzyme activity was found in fractions 10−18, presenting its maximum in fraction 15 (Fig. 2a). To confirm that this diaphorase activity corresponds to the FNR enzyme, we conducted an immunoblot analysis in a replica of the fractions using antibodies against *A. maxima*-FNR, resulting in positive bands, with an approximate mass of 40 kDa, in fractions 13 to 16. Mass spectrometry was also useful to search for the presence of FNR in the membrane. It was detected in 5 bands of Fr 14 (Fig. 3b). In this fraction, we also identified cytochromes b_6 and *f* of the b_6f complex (Table 7).

3.5. Characterization of divinyl chlorophylls by absorption spectra and mass spectrometry

Fig. 4a shows the RP-HPLC profile of chromophores in the methanol extract from MIT9313 thylakoids. Using solvent gradients from polar to less-polar, five main peaks were detected at 460 nm (Fig. 4a). Absorption spectra from a diode-array detector in RP-HPLC were used to identify the chromophore in each peak. ESI MS/MS was applied to confirm the identity of Chls a_2 and b_2 (Fig. 4c and d). Pigments eluted at 13.7 and 18.2 min showed the absorption spectra of Chl a_2 and Chl b_2, respectively. DV-Chl-containing fractions were collected, dried, and suspended in acetone 80%. The visible absorption spectra of both DV-Chls are shown in Fig. 4b. Based on values reported by Shedbalkar and Rebeiz [44] we determine the concentration of each DV-Chl and used that concentration to obtain the molar extinction coefficients (ε) for all wavelengths of Chl a_2 and Chl b_2 (Fig. 4b).

https://doi.org/10.1016/j.heliyon.2018.e01100

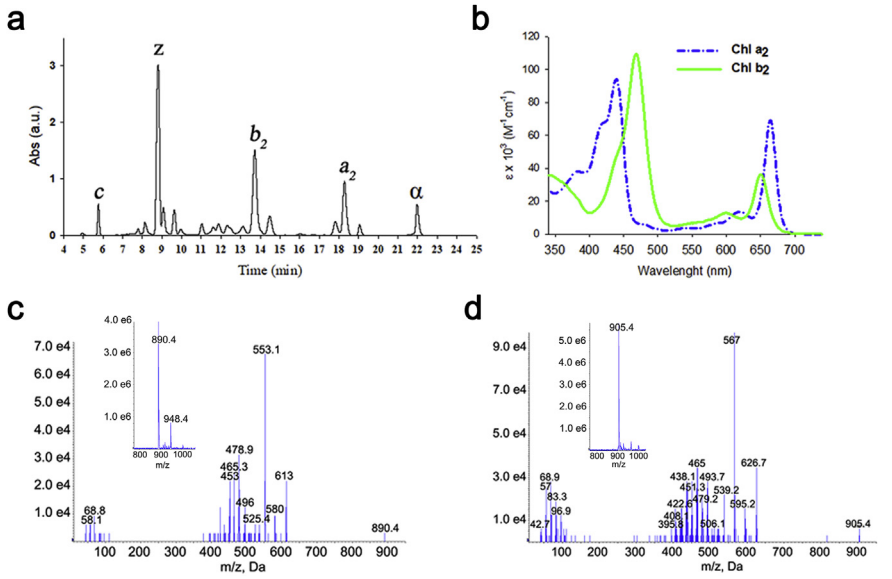

Fig. 4. Characterization and identification of membrane pigments from *Prochlorococcus marinus* MIT 9313. a. Pigment separation from membrane-methanol extract by RP-HPLC. The elution profile was plotted at 460 nm. The elution profile was monitored from 340-740 nm. The absorption spectra of peaks allow us to tentatively identify the components: *c*, [3, 8-Divinyl]-Protochlorophyllide or chlorophyll *c*-like; z, zeaxanthin; b_2, Chl b_2; a_2, Chl a_2; α, α-carotene. b. Molar extinction coefficients of divinyl chlorophylls versus wavelength. c. Positive ion fragmentation of 890.4 precursor that corresponds to $[M]^+$ ion for Chl a_2. Insert: Mass spectrum of fraction eluent corresponding to Chl a_2. d. Positive ion fragmentation of 905.4 precursor that corresponds to $[M + H]^+$ ion for Chl b_2. Insert: Mass spectrum of fraction eluent corresponding to Chl b_2.

The Soret/Q_y ratio obtained by Shedbalkar and Rebeiz [44] for Chl a_2 was the same but was different for Chl b_2 (Fig. 4b). The extinction coefficients (ε) of Chl a_2 and Chl b_2 were used to determine the amounts of each DV-Chls in the fractions of the sucrose gradient from MIT9313. The mass spectra of divinyl chlorophylls are shown in Fig. 4c and d. For Chl a_2 samples, the main molecular ion detected was at m/z 890.4 (insert in Fig. 4c), which corresponds to the $[M]^+$ ion of Chl a_2 ($C_{55}H_{70}MgN_4O_5$). Its monoisotopic calculated mass is 890.520.

The spectrum of fragments of m/z 890.4 ion showed peaks at m/z 613, m/z 580, and m/z 553.1 (Fig. 4c) corresponding to Chl a_2 ion, with the losses of the phytyl chain $[M + H\text{-}278]^+$ ion, the methanol group $[M + H\text{-}32]^+$ ion, and the carboxymethyl group $[M + H\text{-}278\text{-}60]^+$ ion, respectively [45]. The presence of the molecular ion at m/z 948.4 (Fig. 4c insert) is explained by the presence of an adduct of Chl a_2 [46]. The fragmentation spectrum showed the patterns of Chl a_2 (data not show). For Chl b_2 samples, the unique ion detected at m/z 905.4 (Fig. 4d insert) corresponds to the $[M + H]^+$ ion of Chl b_2 ($C_{55}H_{68}MgN_4O_6$; monoisotopic mass: 904.4). The MS/MS spectra of m/z 905.4 (Fig. 4d) showed ions corresponding to disruption of the phytyl chain (m/z 626.7), the methanol group (m/z 595.2), and the carboxymethyl group (m/z 567) [45].

https://doi.org/10.1016/j.heliyon.2018.e01100

3.6. The content of Chl a_2 and Chl b_2 of enriched fractions of the photosynthetic apparatus of *Prochlorococcus marinus* MIT9313

Fig. 5a is a representative profile of a sucrose gradient of DDM-solubilized thylakoid membranes of MIT9313. The cells were grown under continuous illumination with a white fluorescent lamp at an intensity of 1.4 μmol of photons m^{-2} s^{-1}. The distribution of Chls a_2 and b_2 in the sucrose gradient was inferred from the spectra of the fractions. Three peaks of DV-Chls absorbing at 651 nm and 681 nm were identified (Figs. 2a, 3a and 5a). The most rapidly sedimenting peak and the middle peak contained PSI. The slowly sedimenting peak had a difference in absorption at 551 nm over 681 nm, which is congruent with the expected enrichment in Chl b_2 of the antenna protein, PcbB.

The sucrose gradients also had a bump between Fr 9−12 containing PSII that was confirmed by SDS-PAGE (Fig. 3b and Table 6). These results allowed us to calculate that approximately of 70% of Chl a_2 and 67% of the Chl b_2 is in PSI (Fr 2−8). On the other hand, we estimated that 18% of Chl a_2 and 23% of Chl b_2 is located at the antenna protein (Fr 13−17). In the pigment profile of the sucrose gradient, we identified three regions corresponding to the components of the photosynthetic apparatus of MIT9313. The first two peaks, (Fr 2 and Fr 6) corresponding to PSI (Fig. 2a), and a bump in the region of Fr 9−12 is an enriched-PSII region (Fig. 3a). Finally, the peak at Fr 14 is in the enriched-PcbB antenna protein region.

We determined the Chls a_2 and b_2 concentration in all fractions. A representative profile of these sucrose gradients is shown in Fig. 5a. We found Chl a_2 and Chl b_2 in all fractions, but the proportion of Chl b_2 was higher than Chl a_2. The ratios

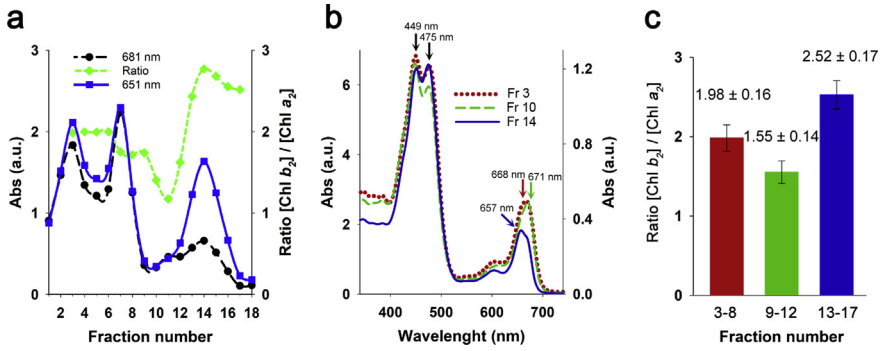

Fig. 5. Distribution of Chls a_2 and b_2 in the enriched fractions of the photosynthetic apparatus of MIT9313. a. Representative pattern of sucrose gradient fractions used to obtain the concentration of Chls a_2 and b_2 of photosynthetic apparatus. The ratio of Chl b_2/a_2 in the fractions is plotted in the sucrose gradient pattern (diamonds). b. Absorption spectra of fractions 3, 10, and 14 representing the regions enriched in PSI, PSII, and light-harvesting substructures, respectively. c. Divinyl chlorophyll composition in enriched fractions of PSI (3−8), PSII (9−12), and light harvesting protein (13−17). The number of Chls a_2 and b_2 determinations derived from five sucrose gradients were: n = 30, for fractions 3−8; n = 20, for fractions (9−12); and n = 30 for fractions 13−17.

https://doi.org/10.1016/j.heliyon.2018.e01100

of Chl b_2/Chl a_2 are shown in Fig. 5a. Three clearly distinguishable ratio levels are observed-these correspond to the three components of the photosynthetic apparatus as defined above. The Chl b_2 rich region corresponds to the antenna component (Fr 13−17) followed by a region (Fr 3−8) of PSI. The region with less Chl b_2 corresponds to the PSII (Fr 9−12).

The spectra of fractions 3, 10 and 14 are shown in Fig. 5b. The absorption spectrum of PSI (Fr 3) shows two maxima at 449 nm and 668 nm with a shoulder at 657 nm indicating the stronger contribution of Chl b_2. The absorption spectrum of PSII (Fr 10) shows two maxima at 449 nm and 671 nm. Finally, the abundance of Chl b_2 in the antenna protein fraction (Fr 14) is shown with three marked maxima at 449, 475 nm and 657 nm. To have an average of the ratio of DV-Chls, we defined the regions: The PSI-enriched fractions with a characteristic peaks of trimer and monomer was defined by Fr 2−8, the PSII-enriched fractions (bump better seen in red circles) was defined by Fr 9−12, and the antenna-enriched region was defined by Fr 13−17. The average ratio of Chl b_2/Chl a_2 for the PSI region was 1.98, 1.55 for PSII, and 2.52 for the light-harvesting antenna (Fig. 5c).

4. Discussion

4.1. Complexes and supercomplexes in the CN-PAGE

The photosynthetic apparatus in MIT9313 is organized in two supercomplexes in complete media: a naked PSI-trimer and a PSII-dimer surrounded by 8 light-harvesting subunits (PcbB). The peripheral antennae in the photosynthetic membranes are two types: associated with the photosystems (fixed antenna) forming supercomplexes or as mobile antenna subjected to light regulation. Under iron depletion, the photosynthetic membranes of MIT9313 have PSI trimers that are surrounded by 18 light-harvesting proteins of PcbA [23]. PSII is a supercomplex formed by a dimeric PSII with up to 8 light-harvesting proteins (PcbB) in both media [23]. We used CN-PAGE to detect and to estimate the quantity of the supercomplexes of the photosynthetic apparatus. The supercomplexes can be extracted and isolated from the photosynthetic membrane and dissociate during the solubilization with detergent and during the centrifugation that precedes the electrophoresis.

The dissociation and diffusion of the subunits of the complexes is limited in the gel, and we explored the distribution of the photosynthetic complexes. We obtained 80% of the DV-Chls bound to the proteins (green bands 1−10) and approximately 50% of them, were bound to the PSI and PSII supercomplexes, (green bands 1−3). The others were associated with the light-harvesting antenna oligomers (Fig. 1a). The more abundant components in the thylakoid membrane of MIT9313 are the proteins of the photosynthetic apparatus as seen in the gels stained with Coomassie blue (Fig. 1b and c). The apparent mass of the supercomplexes in the PSI trimers is 980

https://doi.org/10.1016/j.heliyon.2018.e01100

kDa (calculated 1,080 kDa). For PSII, they were 1,045, 980, and 829 kDa. The calculated mass for PSII dimers with 8 PcbB light-harvesting antennae was 1,196 kDa.

In the two-dimension gels, at least 90% of the core subunits PsaA (A1) and PsaB (A2) characteristic of PSI were in the line corresponding to the apparent mass of 980 kDa (Fig. 1c, band 2). We conclude that all PSI is present *in vivo* as trimers in MIT9313. For PSII, stain intensity of the core subunits CP43 and CP47, and the RC subunits D1 and D2 show that 40% is in the high molecular weight zone of the supercomplexes (Fig. 1 bands 1−3). The remaining PSII appear in bands 4 and 5 of Fig. 1c, which have apparent molecular masses of PSII monomers. The light harvesting capacity of PSII with low level of chlorophylls (about 30 light-harvesting bound in CP43 and CP47) needs to be boosted by the peripheral antenna. We do not anticipate naked PSII dimers much less monomers.

The abundance of the free PcbB subunits of light-harvesting antennae is seen in bands with apparent molecular masses of 192, 152, and 117, which corresponding to dimers, trimers, and tetramers of PcbB. To determine whether all the PSII is present as a supercomplex, we performed analysis with Image Lab software (Suppl. Fig. 4 and Suppl. Table 1). The stoichiometry of free PcbB and CP47 of the monomer according with that analysis was 3.2 (text in Suppl. Fig 4). The conclusion of this speculation is that all PSII is the supercomplex formed by the dimeric PSII and eight PcbB subunits-four in each side of the dimer.

4.2. Cytochrome b_6f complex and ATP synthase in CN-PAGE

The other two membrane complexes of the oxygenic photosynthesis (cytochrome b_6f and ATP synthase) are in relative low abundance versus components of the photosynthetic apparatus, especially the abundant PcbB. However, the components of both complexes were detected by mass spectrometry (Table 4) in the bands 8 and 9 of the CN-PAGE. In the 2-D SDS PAGE, under bands 8 and 9, blue spots at 42, 39, 24 and 18 kDa appeared. These masses correspond to FNR, cytochromes *f* and b_6, and Rieske sulfur protein, respectively (arrows at the right side in Fig. 1c). The components of the cytochrome b_6f complex with highest confidence values were in the 152-kDa band 9. This mass is roughly coincident with that predicted for a cytochrome b_6f dimer. On the other hand, FNR was found with a highest confidence value in the 192-kDa band 8. This finding suggests that the 40-kDa FNR could be associated with cytochrome b_6f dimers.

4.3. Complexes and supercomplexes in sucrose gradients after centrifugation

The approach used to study the biochemical characterization of the complexes and supercomplexes of thylakoid membrane of MIT9313 was the separation of

https://doi.org/10.1016/j.heliyon.2018.e01100

DDM solubilized complexes by sucrose gradient centrifugation (Fig. 2a). Under this condition, we detected the PSI as trimers (fraction 3) and monomers (fraction 6) by measuring the photobleaching of P_{700} (insert of Fig. 2b). The presence of FNR in the gradient was detected by measuring the diaphorase activity (Fig. 2a). To confirm that the diaphorase activity measured corresponded to FNR enzyme, we probed blotted proteins from gradients with an antibody against FNR from *A. maxima* (Fig. 2c). FNR was found in the same fractions presenting diaphorase activity. The PSII core antenna and RC subunits were detected in fractions 9−12 (arrows in Fig. 3a), and their identity was confirmed by mass spectrometry (Table 6). The position suggests that the apparent mass corresponds to a naked monomer of PSII. However, the subunits of the light harvesting antenna (peak at F14) are detected in almost all fractions. Another advantage of using sucrose gradient centrifugation is that Chl a_2 and b_2 contents can be measured.

4.4. The content of Chl a_2 and Chl b_2 in the sucrose fractions

There is a report of extinction coefficients at selected wavelengths of DV-Chls in plants [44]. We actually need contiguous extinction coefficients to obtain the concentration of both DV-Chls by simultaneous equations. The Chls a_2 and b_2 were purified by HPLC (Fig. 4a) and resuspended in acetone at 80%. This solvent was used to extract the pigments from the fractions in the sucrose gradient. Once the Chls a_2 and b_2 were identified by mass spectrometry (Fig. 4c and d), we used the extinction coefficients reported in plants to determine the concentration of each purified DV-Chl. Consequently, we could plot the spectra of both chlorophylls from 340 to 740 nm against their calculated extinction coefficients. We found an abundance of Chl b_2 over Chl a_2 in the proximal antenna of both PSs and, as expected in PcbB, the light-harvesting antenna in MIT9313. The Chl b_2/Chl a_2 ratios were approximately 2, 1.5, and 2.5 for PSI, PSII and PcbB, respectively. There is a precedent study in *Prochlorococcus marinus* MED4: this cyanobacterium grows in the sea surface under high-light intensity and low amount of Chl b_2 is present, and also a small number of harvesting-antenna subunits. On the other hand, in the deeper of euphotic zone, the population shifted to high Chl b_2-containing cells, as in *Prochlorococcus* SS120 [11].

The high content of Chl b_2 in PSI observed in MIT9313 is without precedent. To explain the high content of Chl b_2, we consider that MIT9313 grows, in the deep ocean, where there is low light intensity, which is mostly blue. Red light does not penetrate below 15 m; thus, the deepest waters are enriched with blue light (400−500 nm). The high content of Chl b_2 could be because the absorption band of the DV-Chls is the Soret band The Chl b_2 has better absorption of the blue light due to the red shift in the Soret band relative to Chl a_2.

https://doi.org/10.1016/j.heliyon.2018.e01100

The absence of distal light-harvesting antennae in PSI could be because of the high chlorophyll *a* content in the proximal antenna. In the N-terminal domains of core subunits of the PSI, PsaA-B, which constitute the proximal antenna of PSI there are approximately 80 Chl *a* and the fact that in cyanobacteria PSI is organized as trimer there is an increase of 3 times the Chl content.

In cyanobacteria, the PSI has been crystalized as a homotrimer [47]. The structure of PSI trimers suggest that excitation energy transfer occurs between monomers within the trimer through several connecting pigments [48]. The excitation energy coupling in the trimer will increase the absorption cross section of the antenna for PSI so that an additional antenna for PSI is not needed in most of cyanobacteria. However, *Prochlorococcus* SS120 grows deep in the ocean, with low light intensity. This could explain why this cyanobacterium contains a giant supercomplex consisting of the PSI trimer surrounded by a light-harvesting antenna ring composed of 18-Pcb subunits [49]. This increases the cross section of PSI even further.

In crystals of PSII, it is observed that the core antenna is scarce (CP43 with 14 and CP47 with 16 Chls) per RC. The presence of peripheral antennae is indispensable. In addition, the abundance of Chl b_2 is lower than in PSI probably because the contribution of Chl a_2-rich inner antennae is a bridge in the energy transfer between the light harvesting antenna and the RC. We concluded that PSII is a supercomplex of a dimer of PSII with 8 PcbB light-harvesting antennae that increases the Chl content from 30 per monomer (in the core antenna) to 82 molecules. This in turn increases the optical cross section of the PSII. Moreover, since Chl b_2 has a higher energy level than Chl a_2, the energy transfer between PcbB and the core antennae CP43 and CP 47 may flow from the Chl b_2-rich regions in PcbB to adjacent Chl a_2 regions of the core antennae. The subsequent energy transfer from CP43 or CP47 to the RC occurs via the Chl a_2 regions located within CP43 or CP47.

4.5. Comparison of the content of Chl b_2 in the photosynthetic apparatus of *Prochlorococcus marinus* MIT9313 with the photosynthetic apparatus of other prochlorophyta, green algae and plants

Versus other oxygenic photosynthetic organisms, MIT9313 has a higher content of Chl b_2 [15, 30, 50, 51]. The prochlorophytes together with green algae and plants have a peripheral light-harvesting antenna integrated into the membrane that shares the use of chlorophyll *b* in their photosynthetic apparatus. The subunits that constitute the peripheral intrinsic antennae are of two different families: In cyanobacteria, the *pcb* genes encode membrane-intrinsic proteins of six transmembrane helices called chlorophyll-binding proteins (CBP). In plants and green algae, the membrane-intrinsic proteins with three transmembrane helices. In cyanobacteria

https://doi.org/10.1016/j.heliyon.2018.e01100

with PBSs as a peripheral light-harvesting antenna, the core or proximal antenna of the PSs contain Chl *a* as the harvesting pigment.

The special case of MIT9313 with high relative content of Chl b_2 is without precedent. In *Prochlorophyta* a green cyanobacteria with integral membrane protein as a peripheral light harvesting antenna, the core or proximal antenna of the PSs contains Chl *b* or b_2 in addition to Chl *a* or a_2. In *P. didemi* thylakoids, the Chl *a/b* ratio was close to 5 and the Chl *a/b* ratio for the Pcb-rich fraction was 3 [27]. In *P. hollandica,* the pigment molar ratio of purified PcbC antenna was calculated to be 17 Chl *a*: 4 Chl b [29]. The peripheral antenna formed by PcbB contains more Chl b_2 than the core antenna formed by CP43 and CP47 in *Prochlorococcus* [11].

In contrast, plants with a core or proximal light-harvesting antenna exclusively contain Chl *a*. The Spinach PSII-LHCII supercomplex contains one trimeric and two monomeric LHCIIs. At the outer region of the core, one LHCII trimer and one CP26 monomer flank the side near CP43 and one CP29 is associated with CP47. LHCIIs CP29 and CP26 contain both Chl *a* and Chl *b* [31]. Pea PSI subunits contain only 98 Chl a; Lhca1 has 12 Chl *a* and 2 Chl *b*; Lhca2 Chl *a* has 9 and 5 Chl *b*; Lhca3 has 13 Chl *a* and 1 Chl *b*; Lhca4 has 11 Chl *a* and 4 Chl *b* [32].

4.6. The prevalence of the FNR at the cytoplasmic surface of the thylakoid membrane in cyanobacteria

Analysis of the *Prochlorococcus* SS120 genome showed that a *pet*H gene encodes a FNR of three domains. The N-terminal domain contains a sequence that predicts a transmembrane helix, and consequently a membrane bound protein [24]. In this investigation, we have established the tethering of FNR to the thylakoid membrane in *Prochlorococcus* MIT9313. These results are based on the following: 1) Diaphorase activity was detected in the sucrose gradient centrifugation fractions of solubilized thylakoids from MIT9313 (Fig. 2a). 2) An immunoblot reaction was performed on a SDS-PAGE of the MIT9313 membrane with *A. maxima* FNR antibody resulting in a positive band with an apparent molecular mass of 40 kDa (Fig. 2c), which agree with the predicted mass of PetH 40.9 kDa. 3) In the bands 6−10 of the CN-PAGE of solubilized thylakoids from MIT9313 (Fig. 1b), we detect the presence of FNR by mass spectrometry analysis (Tables 3 and 4).

We then extended the amino acid alignment and hydrophobic analysis to 10 FNR sequences of *Prochlorococcus* spp. and found the preservation of the sequence that defines the transmembrane helix (Suppl. Fig. 2c). Cyanobacteria have been classified in 4 groups, only three species have a gene encoding a two domain FNR (FNR-2D). In the other three groups, FNRs have an N-terminal extension in comparison with the FNR-2D. This N-terminal extension directs the FNR to the PBS in two of the groups [52]. The remaining group is *Prochlorococcus*

https://doi.org/10.1016/j.heliyon.2018.e01100

spp. described here where the N-terminal domain directs the enzyme into the membrane.

Thus, we wonder about the meaning of the prevalence of the FNR on the cytoplasmic surface of the thylakoid membrane in cyanobacteria. Three possible non-exclusive answers can be proposed:1) The interaction of enzymes in the complexes may facilitate the product-substrate channeling or at least the proximity between serial enzymes in order to make the metabolic processes more efficient. In the tripartite model PSI, the source of reduced ferredoxin (Fd) and the PBS are close. 2) Two-dimensional diffusion of Fd to target the FNR is dependent of the interactions of the Fd with the surface of the membrane lipids. A more rapidly skating mode is constrained by the negative charge of the lipids with the anionic Fd. 3) The tethering of FNR to the distal ends of the peripheral rods of PBS near the thylakoid membrane might also facilitate its involvement in PSI-mediated cyclic electron transport [26].

5. Conclusions

The present study shows how Chl a_2 and Chl b_2 are distributed in the photosynthetic apparatus and where FNR is localized in *Prochlorococcus* MIT9313, a cyanobacterium without phycobilisomes. By using CN-PAGE and sucrose gradient centrifugation, together with SDS-PAGE and mass spectrometry, we provide evidence of the abundance in Chl b_2 in the entire photosynthetic apparatus and that the FNR is present in thylakoid membranes. The higher penetration of blue light into the ocean water could explain the unusual abundance of Chl b_2 in both PSII-PcbB and PSI-trimers of this deep-ocean dwelling cyanobacterium. Finally, FNR was shown to be located in thylakoid membranes, as predicted by its N-terminal transmembrane domain. Its possible association with the cytochrome b_6f complex suggests that FNR could participate in cyclic photophosphorylation [26].

Declarations

Author contribution statement

Carlos Gómez-Lojero: Conceived and designed the experiments; Analyzed and interpreted the data; Wrote the paper.

Jesús Barrera-Rojas: Performed the experiments; Analyzed and interpreted the data; Wrote the paper.

Luis González de la Vara: Analyzed and interpreted the data; Contributed reagents, materials, analysis tools or data; Wrote the paper.

Emmanuel Ríos-Castro, Lourdes E. Leyva Castillo: Contributed reagents, materials, analysis tools or data.

https://doi.org/10.1016/j.heliyon.2018.e01100

Funding statement

This work was supported by intramural funds, Centro de investigación y Estudios avanzados (Cinvestav-IPN). JBR received a scholarship from Consejo Nacional de Ciencia y Tecnología (Conacyt), scholarship no. 261984.

Competing interest statement

The authors declare no conflict of interest.

Additional information

Supplementary content related to this article has been published online at https://doi.org/10.1016/j.heliyon.2018.e01100.

Acknowledgements

This paper is dedicated to the memory of Dr. David W. Krogmann, professor colleague and friend. We Thank Dr Marco Antonio Meraz Ríos for his discussions and support in acquisition of materials and reagents. For Jorge Zarco Mendoza about his technical assistance. We also thank to Mrs Leticia Gómez Sandoval for her secretarial assistance.

References

[1] C.S. Ting, G. Rocap, J. King, S.W. Chisholm, Cyanobacterial photosynthesis in the oceans: the origins and significance of divergent light-harvesting strategies, Trends Microbiol. (2002).

[2] R. Croce, H. van Amerongen, Natural strategies for photosynthetic light harvesting, Nat. Chem. Biol. 10 (7) (2014) 492−501.

[3] A.N. Glazer, Light guides. Directional energy transfer in a photosynthetic antenna, J. Biol. Chem. 264 (1) (1989) 1−4.

[4] R.A. Lewin, N.W. Withers, Extraordinary pigment composition of a prokaryotic alga, Nature 256 (1975) 735−737.

[5] T. Burger-Wiersma, M. Veenhuis, H.J. Korthals, C.C.M. Van De Wiel, L.R. Mur, A new prokaryote containing chlorophylls a and b, Nature 320 (6059) (1986) 262−264.

[6] S.W. Chisholm, R.J. Olson, E.R. Zettler, R. Goericke, J.B. Waterbury, N.A. Welschmeyer, A novel free-living prochlorophyte abundant in the oceanic euphotic zone, Nature 334 (6180) (1988) 340−343.

[7] R. Goericke, D. Repeta, Chlorophylls a and b and divinyl chlorophylls a and b in the open subtropical North Atlantic Ocean, Mar. Ecol. Prog. Ser. 101 (1993) 307–313.

[8] R. Goericke, N.A. Welschmeyer, The marine prochlorophyte *Prochlorococcus* contributes significantly to phytoplankton biomass and primary production in the Sargasso Sea, Deep Sea Res. 40 (11) (1993) 2283–2294.

[9] H.A. Bouman, Oceanographic basis of the global surface distribution of *Prochlorococcus* ecotypes, Science 312 (5775) (2006) 918–921.

[10] Z.I. Johnson, Niche partitioning among *Prochlorococcus* ecotypes along ocean-scale environmental gradients, Science 311 (5768) (2006) 1737–1740.

[11] F. Partensky, W.R. Hess, D. Vaulot, *Prochlorococcus*, a marine photosynthetic prokaryote of global significance, Microbiol. Mol. Biol. Rev. 63 (1) (1999) 106–127.

[12] M.L. Coleman, S.W. Chisholm, Code and context: *Prochlorococcus* as a model for cross-scale biology, Trends Microbiol. (2007).

[13] W.R. Hess, G. Rocap, C.S. Ting, F. Larimer, S. Stilwagen, J. Lamerdin, S.W. Chisholm, The photosynthetic apparatus of *Prochlorococcus*: insights through comparative genomics, Photosynth. Res. 70 (1) (2001) 53–71.

[14] Z. Johnson, M.L. Landry, R.R. Bidigare, S.L. Brown, L. Campbell, J. Gunderson, C. Trees, Energetics and growth kinetics of a deep *Prochlorococcus* spp. population in the Arabian Sea, Deep Sea Res. Part II Top. Stud. Oceanogr. 46 (8–9) (1999) 1719–1743.

[15] L.R. Moore, R. Goericke, S.W. Chisholm, Comparative physiology of *Synechococcus* and *Prochlorococcus*: influence of light and temperature on growth, pigments, fluorescence and absorptive properties, Marine Ecol. Progr. Ser. 116 (1995) 259–275.

[16] M. Şener, J. Strümpfer, J. Hsin, D. Chandler, S. Scheuring, N. Hunter, K. Schulten, Förster energy transfer theory as reflected in the structures of photosynthetic light harvesting systems, ChemPhysChem 12 (3) (2012) 518–531.

[17] L.R. Moore, G. Rocap, S.W. Chisholm, Physiology and molecular phylogeny of coexisting *Prochlorococcus* ecotypes, Nature 393 (6684) (1998) 464–467.

[18] G. Rocap, F.W. Larimer, J. Lamerdin, S. Malfatti, P. Chain, N.A. Ahlgren, S.W. Chisholm, Genome divergence in two *Prochlorococcus* ecotypes reflects oceanic niche differentiation, Nature 424 (6952) (2003) 1042–1047.

https://doi.org/10.1016/j.heliyon.2018.e01100

[19] E. Urbach, D.J. Scanlan, D.L. Distel, J.B. Waterbury, S.W. Chisholm, Rapid diversification of marine picophytoplankton with dissimilar light- harvesting structures inferred from sequences of *Prochlorococcus* and *Synechococcus* (cyanobacteria), J. Mol. Evol. 46 (2) (1998) 188−201.

[20] P.M. Shih, D. Wu, A. Latifi, S.D. Axen, D.P. Fewer, E. Talla, C.A. Kerfeld, Improving the coverage of the cyanobacterial phylum using diversity-driven genome sequencing, Proc. Natl. Acad. Sci. U. S. A. 110 (3) (2013) 1053−1058.

[21] J. La Roche, G.W. van der Staay, F. Partensky, A. Ducret, R. Aebersold, R. Li, B.R. Green, Independent evolution of the prochlorophyte and green plant chlorophyll a/b light-harvesting proteins, Proc. Natl. Acad. Sci. U. S. A. 93 (December 1996) (1996) 15244−15248.

[22] S. Satoh, A. Tanaka, Identification of chlorophyllide a oxygenase in the *Prochlorococcus* genome by a comparative genomic approach, Plant Cell Physiol. 47 (12) (2006) 1622−1629.

[23] T.S. Bibby, I. Mary, J. Nield, F. Partensky, J. Barber, Low-light-adapted *Prochlorococcus* species possess specific antennae for each photosystem, Nature 424 (6952) (2003a) 1051−1054.

[24] A. Dufresne, M. Salanoubat, F. Partensky, F. Artiguenave, I.M. Axmann, V. Barbe, W.R. Hess, Genome sequence of the cyanobacterium *Prochlorococcus marinus* SS120, a nearly minimal oxyphototrophic genome, Proc. Natl. Acad. Sci. U. S. A. 100 (17) (2003) 10020−10025.

[25] W.M. Schluchter, D.A. Bryant, Molecular characterization of ferredoxin-NADP+ oxidoreductase in cyanobacteria: cloning and sequence of the petH gene of *Synechococcus* sp. PCC 7002 and studies on the gene product, Biochemistry 31 (12) (1992) 3092−3102.

[26] C. Gómez-Lojero, B. Pérez-Gómez, G. Shen, W.M. Schluchter, D.A. Bryant, Interaction of ferredoxin:NADP+ oxidoreductase with phycobilisomes and phycobilisome substructures of the cyanobacterium *Synechococcus* sp. strain PCC 7002, Biochemistry 42 (47) (2003) 13800−13811.

[27] T.S. Bibby, J. Nield, M. Chen, A.W.D. Larkum, J. Barber, Structure of a photosystem II supercomplex isolated from Prochloron didemni retaining its chlorophyll a/b light-harvesting system, Proc. Natl. Acad. Sci. U. S. A. (2003b).

[28] M. Chen, T.S. Bibby, J. Nield, A.W.D. Larkum, J. Barber, Structure of a large photosystem II supercomplex from *Acaryochloris marina*, FEBS Lett. 579 (2005).

https://doi.org/10.1016/j.heliyon.2018.e01100

[29] M. Herbstová, R. Litvín, Z. Gardian, J. Komenda, F. Vácha, Localization of Pcb antenna complexes in the photosynthetic prokaryote *Prochlorothrix hollandica*, Biochim. Biophys. Acta Bioenerg. (2010).

[30] L. Garczarek, G.W.M. Van Der Staay, J.C. Thomas, F. Partensky, Isolation and characterization of photosystem I from two strains of the marine oxychlorobacterium Prochlorococcus, Photosynth. Res. 56 (2) (1998) 131−141.

[31] X.P. Wei, X.Z. Zhang, X.D. Su, P. Cao, X.Y. Liu, M. Li, Z.F. Liu, Cryo-EM structure of spinach PSII-LHCII supercomplex at 3.2 Angstrom resolution, Nature 534 (2016) 69−74.

[32] X. Qin, M. Suga, T. Kuang, J.R. Shen, Structural basis for energy transfer pathways in the plant PSI-LHCl supercomplex, Science 348 (2015) 989−995.

[33] I. Wittig, M. Karas, H. Schägger, High resolution clear native electrophoresis for in-gel functional assays and fluorescence studies of membrane protein complexes, Mol. Cell. Proteomics 6 (7) (2007) 1215−1225.

[34] I. Wittig, T. Beckhaus, Z. Wumaier, M. Karas, H. Schägger, Mass estimation of native proteins by blue native electrophoresis, Mol. Cell. Proteomics 9 (10) (2010) 2149−2161.

[35] D.I. Arnon, Copper enzymes in isolated chloroplasts. Polyphenoloxidase in beta vulgaris, Plant Physiol. 24 (1) (1949) 1−15.

[36] B. Pérez-Gómez, G. Mendoza-Hernández, T. Cabellos-Avelar, L.E. Leyva-Castillo, E.B. Gutiérrez-Cirlos, C. Gómez-Lojero, A proteomic approach to the analysis of the components of the phycobilisomes from two cyanobacteria with complementary chromatic adaptation: Fremyella diplosiphon UTEX B590 and Tolypothrix PCC 7601, Photosynth. Res. (2012).

[37] A. Shevchenko, O.N. Jensen, A.V. Podtelejnikov, F. Sagliocco, M. Wilm, O. Vorm, M. Mann, Linking genome and proteome by mass spectrometry: large-scale identification of yeast proteins from two dimensional gels, Proc. Natl. Acad. Sci. U. S. A. 93 (25) (1996) 14440−14445.

[38] M.M. Nowaczyk, R. Hebeler, E. Schlodder, H.E. Meyer, B. Warscheid, M. Rogner, Psb27, a cyanobacterial lipoprotein, is involved in the repair cycle of photosystem II, Plant Cell Online 18 (11) (2006) 3121−3131.

[39] H. Liu, R.Y.-C. Huang, J. Chen, M.L. Gross, H.B. Pakrasi, Psb27, a transiently associated protein, binds to the chlorophyll binding protein CP43 in photosystem II assembly intermediates, Proc. Natl. Acad. Sci. U. S A. 108 (45) (2011) 18536−18541.

 https://doi.org/10.1016/j.heliyon.2018.e01100

[40] H. Liu, J.L. Roose, J.C. Cameron, H.B. Pakrasi, A genetically tagged Psb27 protein allows purification of two consecutive photosystem II (PSII) assembly intermediates in synechocystis 6803, a cyanobacterium, J. Biol. Chem. 286 (28) (2011) 24865−24871.

[41] A. Wilde, K. Lünser, F. Ossenbühl, J. Nickelsen, T. Börner, Characterization of the cyanobacterial ycf37: mutation decreases the photosystem I content, Biochem. J. 357 (2001) 211−216.

[42] U. Dühring, K.D. Irrgang, K. Lünser, J. Kehr, A. Wilde, Analysis of photosynthetic complexes from a cyanobacterial ycf37 mutant, Biochim. Biophys. Acta Bioenerg. 1757 (1) (2006) 3−11.

[43] C. Gómez-Lojero, L.E. Leyva-Castillo, P. Herrera-Salgado, J. Barrera-Rojas, E. Ríos-Castro, E.B. Gutiérrez-Cirlos, Leptolyngbya CCM 4, a cyanobacterium with far-red photoacclimation from Cuatro Ciénegas Basin, México, Photosynthetica 56 (1) (2018) 1−12.

[44] V.P. Shedbalkar, C.A. Rebeiz, Chloroplast biogenesis: determination of the molar extinction coefficients of divinyl chlorophyll a and b and their pheophytins, Anal. Biochem. 207 (2) (1992) 261−266.

[45] C. Juin, A. Bonnet, E. Nicolau, J.B. Bérard, R. Devillers, V. Thiéry, L. Picot, UPLC-MSE profiling of phytoplankton metabolites: application to the identification of pigments and structural analysis of metabolites in *Porphyridium purpureum*, Mar. Drugs 13 (4) (2015) 2541−2558.

[46] A. Kruve, K. Kaupmees, Adduct formation in ESI/MS by mobile phase additives, J. Am. Soc. Mass Spectrom. (2017).

[47] P. Jordan, P. Fromme, H.T. Witt, O. Klukas, W. Saenger, N. Krauß, Three-dimensional structure of cyanobacterial photosystem I at 2.5 Å resolution, Nature (2001).

[48] M.K. Şener, S. Park, D. Lu, A. Damjanović, T. Ritz, P. Fromme, K. Schulten, Excitation migration in trimeric cyanobacterial photosystem I, J. Chem. Phys. (2004).

[49] T.S. Bibby, J. Nield, F. Partensky, J. Barber, Oxyphotobacteria: antenna ring around photosystem I, Nature 413 (2001b) 590.

[50] R. Goericke, D.J. Repeta, The pigments of *Prochlorococcus marinus*: The presence of divinylchlorophyll a and b in a marine procaryote, Limnol. Oceanogr. (1992).

[51] H. Komatsu, K. Wada, T. Kanjoh, H. Miyashita, M. Sato, M. Kawachi, M. Kobayashi, Unique chlorophylls in picoplankton *Prochlorococcus* sp.

 https://doi.org/10.1016/j.heliyon.2018.e01100

"Physicochemical properties of divinyl chlorophylls, and the discovery of monovinyl chlorophyll b as well as divinyl chlorophyll b in the species Prochlorococcus NIES-2086", Photosynth. Res. 130 (1−3) (2016) 445−467.

[52] F. Alcántara-Sánchez, L.E. Leyva-Castillo, A. Chagolla-López, L. González de la Vara, C. Gómez-Lojero, Distribution of isoforms of ferredoxin-NADP+ reductase (FNR) in cyanobacteria in two growth conditions, Int. J. Biochem. Cell Biol. 85 (2017) 123−134.

https://doi.org/10.1016/j.heliyon.2018.e01100